Microstructural changes and mass transport in cement-based materials: a modeling approach

A. Michel[a], V. Marcos-Meson[a,b], W. Kunther[a] & M.R. Geiker[c]

[a)] *Technical University of Denmark (DTU), Department of Civil Engineering, Kgs. Lyngby, Denmark*

+45 4525 1656, +45 4588 3282, almic@byg.dtu.dk, http://www.dtu.dk

[b)] *COWI A/S Denmark, Kongens Lyngby, Denmark*

[c)] *Norwegian University of Science and Technology (DTU), Department of Structural Engineering, Trondheim, Norway*

Abstract

A generic modelling framework is presented to relate microstructural changes, *i.e.* changes in the pore volume distribution and phase assemblage, and mass transport in cement-based materials. The modelling framework accounts for mass transport and chemical equilibrium between ions in the pore solution and solid hydrates by means of an extended version of the Poisson-Nernst-Planck equation, in which the chemical equilibrium is solved by the external geochemical code IPHREEQC. Results of numerical studies concerning carbonation and leaching of a cement-based material indicate significant changes in mass transport properties due to chemical reactions leading to alterations in the microstructure. The resulting highly non-linear (both spatial and temporal) microstructural changes are thereby depending on the exposure and indicate that interactions between chemical reactions, pore structure changes, and mass transport have to be accounted for as a whole.

Keywords: *B. Microstructure, B. Pore Size Distribution, B. Thermodynamic Calculations*, C. *Transport Properties, E. Modeling*

1 Introduction

Apart from widely used engineering approaches, which are often limited to *e.g.* describing the ingress of chloride ions as of Fickian diffusion (see *e.g.* [1,2]), in particular, multi-physics modeling tools gained popularity in efforts to assess and predict the service life of cement-based materials. For the numerical solution of the mass transport and chemical equilibrium in cement-based materials, multi-physics modelling approaches often use the finite element method (FEM), see *e.g.* [3–7]. Commonly, state-of-the-art multi-physics models for the assessment and prediction of the service life of cement-based materials employ 'classical' Poisson-Nernst-Planck (PNP) equations to describe the mass transport, *e.g.* transport of ionic species, see *e.g.* [7–9]. The PNP equations describe the mass balance for the considered ionic species along with constitutive assumptions for the corresponding mass flows. In doing so, the assumptions for mass flows of ionic constituents are described by Nernst-Planck relations accounting for the influence of concentration gradients of the ionic species of interest as well as the gradient of the electrical potential [10]. The electrical potential is calculated from Gauss' law applying suitable constitutive assumptions, also referred to as the Poisson equation of electrostatics. The Nernst-Planck equation describing mass flows and the Poisson type of the equation determining the electrical potential are coupled in both directions. The 'classical' PNP equations do not account for fluid motion leading to an advective flow of dissolved ionic species. This limitation can be overcome by extending the 'classical' PNP equations to account for moisture transport.

However, the accuracy of modelling approaches is impaired not only due to simplifying assumptions concerning the processes associated with deterioration, such as chemical equilibrium and transport mechanisms; predictive capabilities are lacking due to absence of important relations between chemical reactions, pore structure changes, and mass transport. Without taking into account these interactions the

predictive capabilities of such modeling approaches will always be limited. The focus of this study was to establish a functional description of relations between pore structure, volume changes, and mass transport to enable modeling of the influence of microstructural changes on the mass transport in cement-based materials. Mass transport in cement-based materials along with chemical equilibrium between ions in the pore solution and solid hydrates was solved by an extended version of the Poisson-Nernst-Planck system of equations, in which the chemical equilibrium was solved by the external geochemical code IPHREEQC [11]. To relate phase changes and mass transport properties, scaling functions based on a mechanistic modeling approach [12,13] taking into account the impact of moisture content and the microstructure of porous media on moisture transport were used. The capability of the multi-physics modeling approach to relate microstructural changes and mass transport properties of cement-based materials was illustrated by two case studies: carbonation and leaching of cement-based materials in saturated condition.

2 Modeling approach

Experimental results reported in the literature (*e.g.* [14–17]) clearly show that exposure can lead to considerable alterations of cement-based materials. These changes include among others effects on the phase assemblage, pore structure, and mass transport properties, which are related to each other. This dependency calls for modelling approaches that entail descriptions of the underlying mechanisms governing mass transport, chemical reactions, and microstructural changes (phase assemblage and pore structure) as well as relations in between these features. Widely used engineering approaches, often limited to *e.g.* describing the ingress of chloride ions as of Fickian diffusion, lack the ability to deal with complex interactions and thus, may lead to inconsistent conclusions regarding deterioration pro-

cesses and durability of cement-based materials as *e.g.* the effective diffusion of chloride ions in carbonated cement paste. Multi-physics modelling approaches, on the other hand, provide the possibility to investigate and simulate the alterations in cement-based systems, while capturing the complexity of microstructure (phase assemblage and pore structure), mass transport, and chemical interactions, see Figure 1.

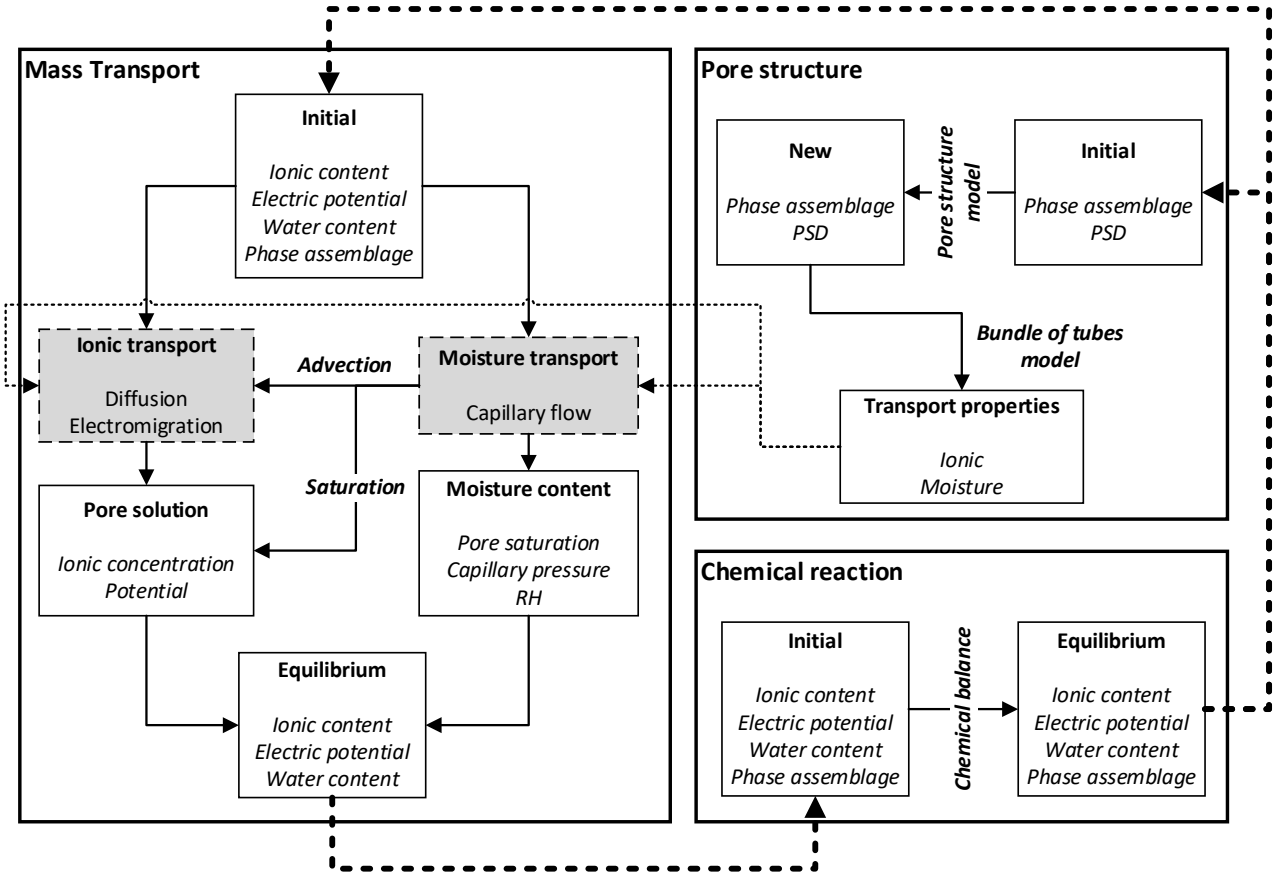

Figure 1: Conceptual relation between microstructure, *i.e.* phase assemblage and pore structure, and mass transport in cement-based materials.

2.1 General framework

In the following, a brief description of the theoretical background of the adapted multi-phase reactive transport model is presented, including the description of mass transport equations and chemical equilibrium suitable for modeling of cement-based materials. A simplified version of the general governing equations obtained from the electroquasistatic Hybrid Mixture Theory (HMT) approach is used to develop a model for a reactive multi-phase flow model for cement-based materials. The transporting phases considered are the liquid water phase including dissolved charged and neutral ionic species and the gas phase, which may include gases, such as CO_2 and/or water vapor. Solid phases and their constituents are considered as one rigid mixture and are only part of the framework in form of chemical interactions with constituents present in the liquid water phase. Chemical reactions are included in the HMT through kinetic source/sink terms in the mass balance equations for the constituents.

For the solution of the highly non-linear mass transport problem, a finite element approach is used, see *e.g.* [18]. The weak form of the governing equations is obtained using the Green-Gauss theorem, while the one-dimensional Galerkin's method is used to discretize the spatial domain with linear elements. Time discretization is carried out using a single parameter implicit time integration scheme. Non-linearity in the model is accounted for applying a modified Newton-Raphson scheme. For more detailed information on implementation, finite element formulation and solution, data coupling, *etc*. reference is made to *e.g.* [6,19–21].

2.2 Governing equations

Mass transport in cement-based materials along with chemical equilibrium between ions in the pore solution and solid hydrates is solved by an extended version of the Poisson-Nernst-Planck (PNP) system

of equations. Within the modeling approach solution of the mass transport is based on the work of Johannesson [10], while chemical interactions are considered as described in *e.g.* [22]. Assuming instantaneous local chemical equilibrium allows for the numerical solution of the chemical equilibrium introducing an operator splitting approach in the transport equation [6]. This approach enables a transient solution of the mass transport while utilizing mass transport results as input for chemical equilibrium calculations. Results of the chemical equilibrium calculations are then used as initial values for the subsequent mass transport calculation. This modeling approach enables the solution of the chemical equilibrium in the spatial domain for all time steps and the governing mass transport equation may then be written as follows:

$$\varepsilon \frac{\partial c_i}{\partial t} + c_i \frac{\partial \varepsilon}{\partial t} = \nabla(D_i \varepsilon \nabla c_i + D_i c_i \nabla \varepsilon - A_i z_i \varepsilon c_i \nabla \Phi) + v\varepsilon \nabla c_i + v c_i \nabla \varepsilon + q_i \qquad (1)$$

where ε is the degree of saturation, c_i is the ionic concentration of species i in the liquid phase, t is the time, D_i is the diffusion coefficient of the ith ionic species, z_i is the valence of the ith ionic species, Φ is the electrical potential, v is the velocity of the liquid phase, and q_i a chemical equilibrium term. The ion mobility, A_i, of the ith ionic species is thereby defined by the Einstein-Smoluchowski equation, *i.e.* $A_i = (F/RT)D_i$, where F is Faraday's constant, R the universal gas constant, and T the absolute temperature. The first and second term on the right-hand side of Eq. 1 describe the standard diffusion part and the effect of moisture gradient changes on the ion concentration, respectively of the fully coupled problem. The third term accounts for the effect of diffusion of the ith ionic species due to the development of an electrical potential gradient, while the fourth and fifth term account for advective motion due to moisture gradients. To fulfil a closed system of equations, a relation for the electrical potential is

required. The relation is based on Gauss' law and represents the Poisson part of the equation, which may be described as follows:

$$\xi_d \xi_0 \nabla^2 \Phi = F \sum_{i=1}^{N} c_i^l z_i \tag{2}$$

where ξ_d is the relative dielectricity coefficient and ξ_0 the dielectricity coefficient of vacuum.

2.3 Chemical equilibrium

Chemical equilibrium is considered for reactions among ionic species in the liquid phase, the equilibrium between ionic constituent and the solid cement hydrate phases, and between gaseous constituents in the air-filled space of the porosity and the dissolved constituents of the liquid phase to describe the mass exchange term q_i. For the solution of the chemical equilibrium, the geochemical code IPHREEQC, see *e.g.* [11] is used, in which the chemical equilibrium for the aqueous species may be expressed as follows:

$$V^T \mu^{aq} = 0 \tag{3}$$

where μ^{aq} is the chemical potential vector containing all ions in the aqueous phase and V^T the transposed stoichiometric mass matrix. Each row in the matrix system of Eq. (3) represents a condition for the defined reactions. Once the chemical potentials of the individual constituents have been established, with a proper definition of the reference potentials, the solubility equations of the individual reactions of the system can be obtained. Aqueous reactions in the liquid water phase and the interaction between dissolved ions and solid phases are described in a similar manner as Eq. (3) based on the composition

of the chemical potential of the individual constituent included. The equations for pure mineral dissolution or precipitation are given by classical dissolution reactions in which the activity of the mineral phase is set to a constant reference value. A solid solution phase is assumed to consist of mixed solid phases called end members. The dissolution or precipitation of the end members is thereby dependent on the individual concentration of the end members in the solid solution phase. The equilibrium condition for partial gases in a gas mixture phase (in equilibrium with the aqueous species) may be described as follows:

$$V_g^T(\mu^{aq} - \mu^g) = 0 \tag{4}$$

where μ^g is the chemical potential vector containing all constituents in the gas phase and V_g^T the right-hand side stoichiometric coefficients matrix for the aqueous species participating in all partial gas constituents of the gas mixture.

In the following, the focus is placed on establishing a modeling approach to relate microstructural changes and mass transport; in particular, the dissolution and formation of phases leading to changes in the pore size distribution, which is then linked to the mass transport in cement-based materials. Thus, for more detailed information on the solution of the chemical equilibrium reference is made to *e.g.* [10,19,23].

2.4 Pore structure and moisture transport

Assuming that contributions to the moisture transport due to air transfer, gravity, radiation, liquid transport due to temperature gradients, and effects of the gaseous phase on the moisture and heat storage are negligible as well as temperatures remain below the boiling temperature of water [24], liquid and water vapor moisture transport in porous media may be described as follows, see *e.g.* [25–27]:

$$\frac{\partial m_{l+v}}{\partial t} = -C\frac{\partial p_c}{\partial t} = -\nabla\left(\frac{D_v(\Theta_l)}{R_v T}\nabla p_v + K_l(\Theta_l)\nabla p_c\right) \tag{5}$$

where, m_{l+v} is the sum of the water vapour and liquid water content, C the moisture capacity, p_c the capillary pressure, D_v the vapour diffusion coefficient, θ_l the moisture content, R_v the gas constant of water vapour, T the temperature, p_v the vapour pressure, K_l the liquid conductivity coefficient, and t the time. Using Kelvin equation and capillary pressure, p_c, as the common driving potential for vapor and liquid water transport, Eq. 5 yields:

$$\frac{\partial m_{l+v}}{\partial t} = -C\frac{\partial p_c}{\partial t} = -\nabla\left(\frac{D_v(\Theta_l)}{R_v T}\frac{p_{v,sat}\phi}{\rho_l R_v T}\nabla p_c + K_l(\Theta_l)\nabla p_c\right) \tag{6}$$

where $p_{v,sat}$ is the saturation vapor pressure, ρ_l the density of liquid water, and φ the relative humidity. Eq. 6 and 1 are coupled through determination of the degree of saturation, ε, obtained from the mass flow rate, $\frac{\partial m_{l+v}}{\partial t}$, as well as the flow velocity, ν.

The cornerstone of the proposed modeling approach is a functional description of relations between pore structure, volume changes, and mass transport to enable modeling of the influence of microstructural changes on the mass transport in cement-based materials. The pore structure, *i.e.* the pore volume distribution or moisture storage characteristic, is described by a weighted sum of Gauss cumulative distribution functions in the present modeling approach [28], see Figure 2. While the moisture storage function is described by Eq. 7, the pore volume distribution as its derivative is given by Eq. 8. Capillary pressure, pC, is thereby expressed in a logarithmic scale.

$$\Theta_l(pC) = \sum_{i=1}^{N}\left[\frac{\Delta\Theta_i}{\sqrt{2}}\left(1 + erf\left(\frac{pC_i - pC}{\sqrt{2}S_i}\right)\right)\right] \tag{7}$$

$$\frac{\partial\Theta_l}{\partial pC} = -\sum_{i=1}^{N}\left[\frac{\Delta\Theta_i}{\sqrt{2\pi}S_i} exp\left(-\frac{(pC_i - pC)^2}{2S_i^2}\right)\right] \tag{8}$$

where N is the modality and S the standard deviation. The location of the pore maxima, *i.e.* the inflection points within the moisture storage function, is thereby defined by pC_i, while the slope of these inflection points is governed by S_i. The plateau levels between the different modalities are defined by $\Delta\theta_i$, representing weighting factors for each modality; see Figure 2. Although, alternative multi-modal functional descriptions have been proposed in the literature, see *e.g.* [29,30], the high flexibility (especially for higher modalities), as well as the relation of parameters to measured data, are expedient. In particular, measured sorption and retention data are directly related to the driving potential, *i.e.* water, and thus more reliable for use in pore models compared to data from *e.g.* imaging techniques [31] or mercury intrusion [31,32].

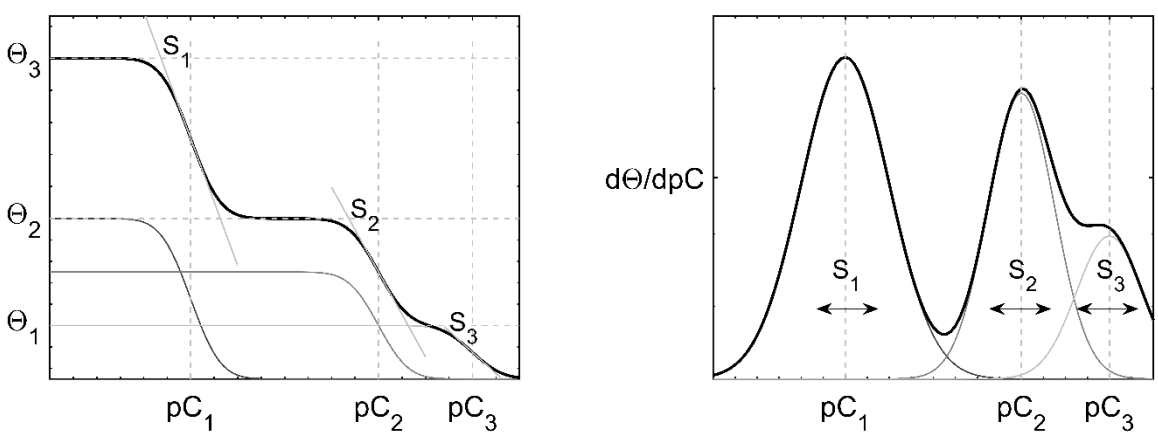

a) b)

Figure 2: a) three-modal moisture storage function and its derivative b) the pore volume distribution, after [12].

2.5 Pore volume changes and mass transport

To account for pore volume related microstructural changes due to dissolution and formation of phases on the mass transport in cement-based materials, the pore structure is represented by a bundle of tubes model, see *e.g.* [26,33]. In that way, length and cross-sectional area of the pores are used to relate incremental pore radii to incremental pore volume. Assuming a unit length, dx, for all pores, the pore radii distribution can be obtained dividing the pore volume distribution by the cross-sectional area, πr^2, as follows:

$$\frac{d\Theta_l}{dr}\frac{1}{\pi r^2} = \frac{dn}{dr} \tag{9}$$

where n is the cumulative number of pores.

To relate environmental-induced changes in the phase assemblage of cement-based materials on the ionic transport, a tortuosity factor, T_n, is introduced, which ranges between zero and one and accounts for effects on the diffusion coefficient, D^i, of each ion as follows:

$$D^i_{eff} = D^i T_k f_l(\Theta_l) \tag{10}$$

where D^i_{eff} is the effective diffusion coefficient of the ith ionic species and $f_l(\Theta_l)$ a scaling function for liquid flow (see Eq. 13). As a first order approximation, the tortuosity factor is recalculated after each determination of the chemical equilibrium and is related to the initial tortuosity factor, T_0, as follows:

$$T_k = T_0 \left[exp\left(log\left(\frac{1}{T_0}\right)\left(1 - \left(\frac{1}{\omega_k/\omega_0}\right)^{\tau}\right)\right)\right] \tag{11}$$

where T_k is the tortuosity factor at time step k, τ a shape factor, ω_k the total porosity at time step k, and ω_0 the initial porosity. It should be noted that T_k approaches one for $\tau > 0$, which means that the effective diffusion coefficient approaches the self-diffusion coefficient of the ith ionic species. Changes in the phase assemblage, and thus the total pore volume (see *e.g.* [34–36]), of the cement-based material, are resolved by means of Eq. 1 as well as the geochemical code IPHREEQC.

To account for environmental-induced changes in the phase assemblage of cement-based materials on the coupled liquid and vapor transport, vapor diffusion and liquid flow scaling functions are introduced, respectively. The applied scaling functions were proposed by Scheffler & Plagge [12] and are based on a mechanistic modeling approach taking into account the impact of moisture content and the microstructure of porous media on moisture transport. The scaling function for vapor diffusion and liquid flow may be written as follows:

$$f_v(\Theta_l) = \frac{1 - \frac{\theta_l}{\omega_k}}{\left(\frac{\theta_l}{\omega_k}\right)^{n_{sp}} + \left(1 - \frac{\theta_l}{\omega_k}\right)^2 \left(1 - \left(\frac{\theta_l}{\omega_k}\right)^{n_{sp}}\right)} \tag{12}$$

$$f_l(\Theta_l) = \frac{\left(\frac{\theta_l}{\omega_k}\right)^{n_{sp}}}{\left(\frac{\theta_l}{\omega_k}\right)^{n_{sp}} + \left(1 - \frac{\theta_l}{\omega_k}\right)^2 \left(1 - \left(\frac{\theta_l}{\omega_k}\right)^{n_{sp}}\right)} \tag{13}$$

where $f_v(\theta_l)$ is the vapor diffusion scaling function, $f_l(\theta_l)$ the liquid flow scaling function, ω_k the total porosity at time step k, and n_{sp} a shape parameter accounting for the serial-parallel connectivity of

pores. More detailed information on the mechanistic model and the derivation of the liquid and vapor flow scaling functions can be found in [12,13]. Vapor flow transport is then described as follows in the present modeling approach:

$$D_v(\Theta_l) = \frac{D_{v,air}}{\mu_{dry}} f_v(\Theta_l) \tag{14}$$

where $D_{v,air}$ is the vapor diffusion coefficient of air and μ_{dry} the vapor diffusion resistance number. The vapor diffusion coefficient of air is given as follows according to the relation provided in [37]:

$$D_{v,air} = 0.083 \frac{p_0}{p} \left(\frac{T}{273.15}\right)^{1.81} \tag{15}$$

where p_0 is the reference gas pressure. The liquid moisture flow is described as follows in the present modeling approach:

$$K_l(\Theta_l) = \begin{matrix} K_{l,cap}(\Theta_l) \\ K_{l,sat}(\Theta_l) \end{matrix} \; if \; \begin{matrix} \Theta_l \leq \Theta_{cap} \\ \Theta_l > \Theta_{cap} \end{matrix} \tag{16}$$

where $K_{l,sat}$ is the saturation conductivity, θ_{cap} the capillary saturation, and $K_{l,cap}$ the liquid conductivity in the capillary range, which is described as follows:

$$K_{l,cap}(\Theta_l) = K_{l,hyg}(\Theta_l) + n_{cap} K_{eff} f_l(\Theta_l) K_{l,rel}(\Theta_l) \tag{17}$$

where $K_{l,hyg}$ is hygroscopic liquid conductivity, n_{cap} a scaling parameter to adjust the conductivity function in the higher moisture content range, K_{eff} the effective liquid conductivity, and $K_{l,rel}$ the relative liquid conductivity containing information on the pore structure of the porous media. For the determination of the relative liquid conductivity the approach derived by Mualem [38] is employed:

$$K_{l,rel}(\Theta_l) = \left[\frac{\int_0^{\Theta_l} p_c\,(\theta)^{-1} d\theta}{\int_0^{\omega_k} p_c(\theta)^{-1}\, d\theta}\right]^2 \tag{18}$$

Dependencies of the vapor diffusion and liquid flow scaling function, see Eq. 12 and 13, as well as effective and relative liquid conductivity, see Eq. 17 and 18, on the total porosity allow for accounting of the effects of phase assemblage changes by means of Eq. 1 as well as the geochemical code IPHREEQC. Volume changes may thereby be discretely distributed to the pore volume distribution after the volume of dissolved or newly formed phases is determined, see *e.g.* [34–36]. It is thereby assumed that the relation between the shape parameter n_{sp} accounting for the serial-parallel connectivity of pores and incremental changes in the pore volume distribution at time step k, $\Delta\omega_k$, is sufficiently described by a simple rational function, *i.e.* $1/\Delta\omega_k$. Similar dependencies are assumed for the capillary sorption coefficient n_{cap} and the vapor diffusion resistance number μ_{dry}. Finally, the impact on the effective conductivity K_{eff} is accounted for by a power law, *i.e.* $\Delta\omega_k^4$ according to the Hagen-Poiseuille equation.

3 Case studies

To demonstrate the applicability of the presented modeling approach to account for the interactions between phase assemblage and porosity changes as well as mass transport properties of cement-based materials, two numerical examples are presented in the following. Results of the numerical examples are compared to experimental observations presented in the literature. The focus was placed on experimental observations related to microstructural changes, in particular changes in the pore volume distribution due to formation or dissolution of phases. However, it should be noted that the objective of the

numerical examples was to reproduce overall trends and deterioration mechanisms observed in the experimental studies as the lack of input parameters and implemented first order modelling assumptions (see *e.g.* Eq. 10 and 11) did not allow for full reproduction of the experimental observations.

Among others, the selected thermodynamic database for the chemical reactions has a considerable impact on the results. In the present approach, the *Cemdata18* thermodynamic database (in form of a PHREEQC format database provided for download from http://www.empa.ch/cemdata) was used [39]. In addition, supplementary aqueous, gaseous, and solid species were selected from the GEMS version of the PSI/Nagra thermodynamic database [40]. An overview of the pure solid-phases and solid-solutions considered for the following examples is given in Table A 1. The C–S–H phase in the model is thereby approximated by means of an solid-solution as described in [41]. The C–S–H solid-solution has six end-members, which are governed by the dissolution reactions and solubility constants given in Table A 2. The solid-solution coexists with SiO_2 at C/S < 0.67 and with $Ca(OH)_2$ at C/S > 1.7. Diffusion coefficients for all ions considered in the examples were based on standard values for self-diffusion (see Table A 3) and subsequently adjusted by the tortuosity factor according to Eq. 11. Chemical shrinkage and self-desiccation were not considered, *i.e.* full saturation was assumed for all case studies.

3.1 Leaching

The presence of solutions less concentrated than the pore solution in contact with the hardened cement matrix will dissolve constituents of the cement paste and lead to leaching. Despite the fact that there are a number of studies investigating the extent of leaching (in particular Ca leaching) as well as impacts on mechanical behavior in cement-based materials, see *e.g.* [42–45], only a few studies focused on microstructural changes including effects on transport properties, see *e.g.* [14,46,47]. Among the few studies that explored microstructural alterations due to leaching, Gallé *et al.* [14] conducted studies to

examine the development of water permeability with respect to the degradation state. Accelerated leaching tests were carried out on pure hardened cement paste and concrete measuring water permeability as well as undertaking pore structure analysis by means of mercury intrusion porosimetry to quantify the impact of leaching. Results presented in [14] indicate that leaching caused the formation of additional capillary porosity (0.1 – 1 μm) and was responsible for a significant increase in total porosity (around 90 %) due to the dissolution of portlandite as well as C-S-H decalcification, see Figure 3. At the same time, results presented in [14] indicate a considerable increase in water permeability by about two orders of magnitude for cement paste as well as concrete specimens. Gallé *et al.* [14] found thereby a good correlation between the observed increase in water permeability and porosity. Similar results were reported in [15] by Phung *et al.*, who conducted accelerated leaching experiments on cement paste samples with different water-binder-ratios (w/b) and limestone filler replacement ratios. Microstructural and mineralogical changes after exposure to ammonium nitrate solution were characterized by scanning electron microscopy, X-ray diffraction, mercury intrusion porosimetry, ion chromatography, and nitrogen adsorption. Results presented in [15] showed considerable alteration of the microstructure due to leaching, including higher specific surface area, increased total porosity, and a shift to larger pore sizes. Phung *et al.* observed considerably higher effects on the micro-pore volume compared to the mesopore volume, which was attributed to leaching of C-S-H, due to the larger volume fraction compared to portlandite.

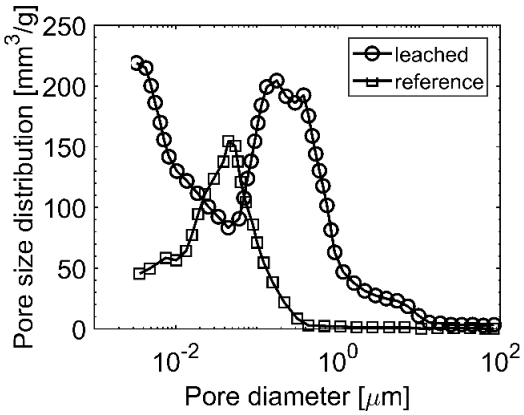

Figure 3: Microstructural changes due to leaching in cement paste measured by combined mercury intrusion porosimetry and nitrogen adsorption within 3 mm from the exposed surface, data reproduced from [15].

To demonstrate the capabilities of the modelling approach, exposure of a cement-based matrix to pure water with a pH of five is assumed simulating the dissolution and leaching of cement constituents. The objective of the simulations was thereby to reproduce trends reported in the literature, rather than fitting the experimental data. In total 90 elements were used in this 1D simulation to discretize a 300 mm domain with a finer mesh in the vicinity of the exposed node (surface). The simulation time was 50 years during which the chemical equilibrium was determined every five days. The oxide composition of an ordinary Portland cement (see Table 1) was used initially to determine the chemical composition of solid and liquid components using the thermodynamic database provided in Table A 1. Additional model parameters describing the mass transport as well as pore volume distribution, are given in Table 2.

Modelling results illustrating the phase assemblage, ionic concentration, and elemental composition after 50 years of exposure are shown in Figure 4. The presented results indicate that the model is able to reproduce the governing deterioration mechanism, *i.e.* essentially a leaching of calcium hydroxide

and a progressive decalcification of C-S-H, as reported previously [14,15]. Upon calculation of the volume of leached or dissolved phases, the impact of exposure on the pore volume distribution can be determined. Figure 5 illustrates changes in the pore volume distribution at a distance of 5 mm from the node in contact with the exposure solution. It is assumed that 70 % of the pore volume changes are attributed to gel pores, while 25 % and 5 % are attributed to capillary and macro pores, respectively; *i.e.* the majority of the microstructural changes are affecting gel pores compared to capillary and macro pores as *e.g.* reported in [15]. Results presented in Figure 5, indicate that the modelling approach is able to reproduce trends in the experimental observations reported previously in the literature (see Figure 3). In particular, increased total porosity as well as the shift to larger pore sizes with considerably higher effects on the micro-pore volume compared to the mesopore volume are mirrored.

The impact of changes in the pore volume distribution on the mass transport was determined using Eq. 9 to 17. Results of the simulation highlighting the impact of exposure, *i.e.* changes in the pore size distribution due to leaching, on the moisture conductivity as well as ionic diffusion are presented in Figure 6. For the chosen model parameters and assumptions, the results indicate a considerable change in conductivity over the complete moisture range. The largest impact is found at saturation, with an increase in moisture conductivity of around two orders of magnitude; see Figure 6 a). The numerical results are thereby in good agreement with experimental observations reported in *e.g.* [14,15]. Figure 6 b) illustrates the impact of exposure and subsequent microstructural changes on the ionic diffusion by means of the introduced tortuosity factor, see Eq. 10 and 11. Changes in the pore volume distribution result thereby in a considerable increase in ionic diffusion over the complete moisture range.

Table 1: Oxide composition of cement, after [15], with the exception of added CO_2 to account for modern cements.

	CaO	SiO_2	Fe_2O_3	Al_2O_3	SO_3	Cl^-	Na_2O	K_2O	MgO	$CaSO_4$	CO_2
Mass%	63.0	20.0	3.0	5.0	2.9	0.06	0.85	0.9	1.8	1.5	1.0

Table 2: Model parameters for leaching simulation.

Parameter	Symbol	Value	Unit
w/c	w/c	0.40	-
Initial total porosity	ω_0	0.304	m^3/m^3
Initial tortuosity factor (ionic diffusion)	τ	0.10	-
Shape parameter	n_{sp}	1.40	-
Vapor diffusion coefficient of air	$D_{v,air}$	Eq. 15	m^2/s
Vapor diffusion resistance number	μ_{dry}	9	-
Relative liquid conductivity	$K_{l,rel}$	Eq. 17	S
Liquid conductivity at saturation	$K_{l,sat}$	1e-5	S
Modality – pore volume distribution	N	3	-
	S_1	0.55e-2	µm
Standard deviation – pore volume distribution	S_2	0.85	µm
	S_3	0.75e2	µm
	pC_1	1e-2	µm
Pore maxima – pore volume distribution	pC_2	1e0	µm
	pC_3	1e2	µm
	$\Delta\theta_1$	0.168	m^3/m^3
Plateau levels – pore volume distribution	$\Delta\theta_2$	0.131	m^3/m^3
	$\Delta\theta_3$	0.005	m^3/m^3

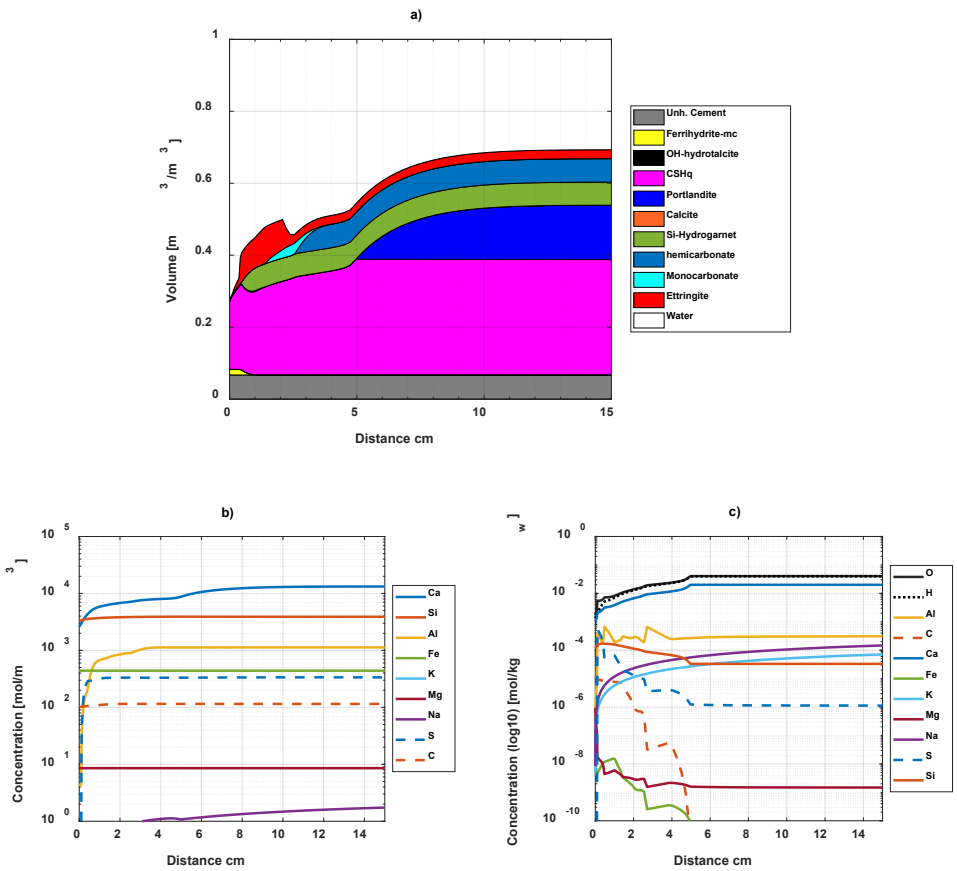

Figure 4: Model results of phase assemblage after 50 years of leaching exposure: a) solid phases, b) elemental composition (per total volume), and c) total aqueous elemental concentrations.

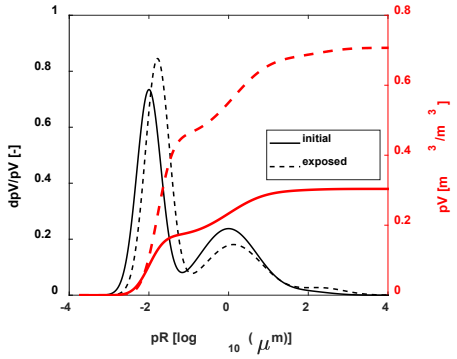

Figure 5: Change in pore size distribution and cumulative pore volume (normalized with respect to total pore volume) at a distance of 5 mm from the exposed node after 50 years of exposure.

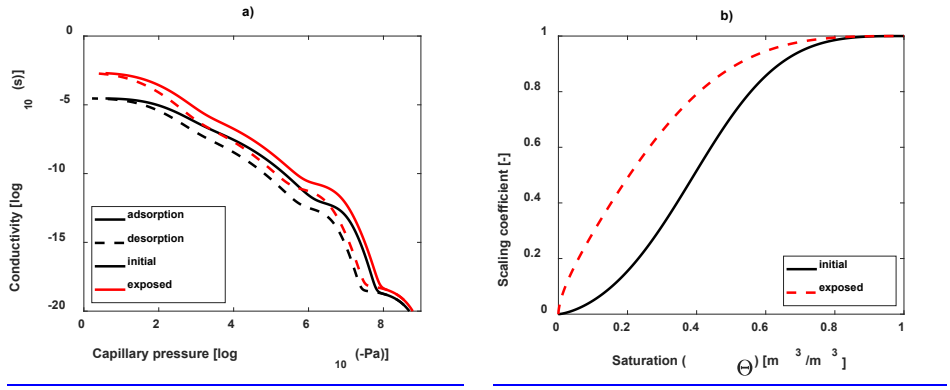

Figure 6: Impact of change in pore size distribution at a distance of 5 mm from the exposed node after 50 years of exposure on a) the moisture conductivity and b) scaling coefficient for ionic diffusion.

3.2 Carbonation in saturated condition

Reaction of carbon dioxide (from the atmosphere or in solution) with calcium bearing cement phases leads to microstructural changes, such as *e.g.* pore size distribution, and porosity, and thus affects the strength and durability of reinforced concrete [48]. Even though a vast amount of studies have focused on investigating phase changes due to carbonation of cement-based materials, see *e.g.* [49–53], as well as effects on the porosity, see *e.g.* [54–56], limited studies dealt with the impact of these on the mass transport. Among the few studies, Houst and Wittmann [17] reported a reduced water absorption in carbonated Portland cement paste compared to non-carbonated samples. Ngala and Page [55] found an increase of around two orders of magnitude for chloride diffusion coefficients in carbonated blended cement pastes. However, the influence of carbonation on the chloride binding capacity was not discussed. Similar results were published by Borges *et al.* in [57] for oxygen diffusivity of carbonated blended cement paste specimens, which was attributed to extensive cracking caused by carbonation. In contrast, Phung *et al.* [16] reported a decrease in water permeability of around one order of magnitude after four weeks of carbonation for both ordinary and blended cement pastes. Contradictions in the experimental

observations may be related to the duration of testing. Initially, a decrease in total porosity is found, which was interpreted to have its origin in the carbonation of portlandite [56]. Upon carbonation of portlandite, an increase in porosity can be observed, which is consequently seen as the carbonation of C-S-H, see Figure 7.

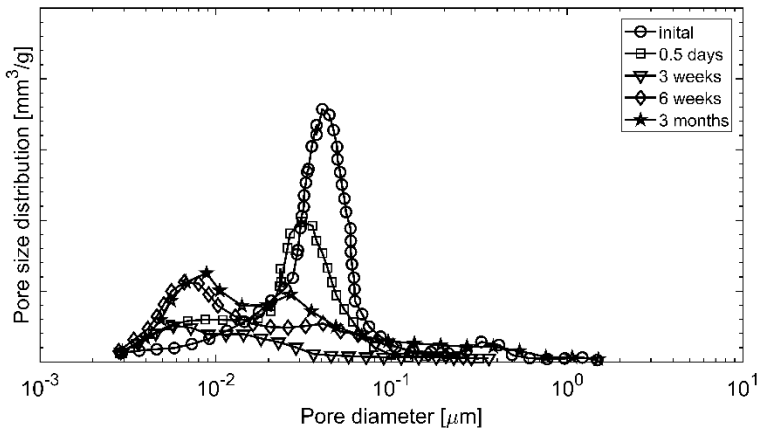

Figure 7: Evolution of the threshold diameter with time estimated from mercury intrusion porosimetry (MIP) on Portland cement samples exposed to CO_2-saturated water up to three months, data reproduced from [56].

To illustrate the ability of the modelling approach, carbonation of a cement-based matrix is modelled by means of exposure to a CO_2 containing solution (0.1 mol/kg$_w$). Composition of the solution was thereby selected to counteract leaching. As for the first example, a 300 mm domain was discretized by 90 elements with a finer mesh near the exposed node. The total simulation time was two years during which the chemical equilibrium was determined every five days. Oxide composition of the cement as well as model parameters are identical to the ones selected for the first example (see Table 1 and Table 2). Moreover, as for the previous example, it is assumed that 70 % of the pore volume changes are attributed to gel pores, while 25 % and 5 % are attributed to capillary and macro pores, respectively. The

shape parameter n_{sp} accounting for the serial-parallel connectivity of the pores, capillary sorption coefficient n_{cap}, the vapor diffusion resistance number μ_{dry}, and effective conductivity K_{eff} are determined in the same manner as previously described.

Results of the modelling approach illustrating the phase assemblage, ionic concentration, and elemental composition after two years of exposure are given in Figure 8. In general, the results show that the model is capable of reproducing the governing phase changes of carbonation, *i.e.* initial dissolution of portlandite followed by decalcification of C-S-H and formation of $CaCO_3$. However, the model also predicts the formation of a considerable amount of ettringite in a region of approximately 2 to 5 mm from the exposed node. This 'artefact' is owed to the imposed boundary conditions, *i.e.* leaching of ions is omitted in the simulation. The stability of the ettringite in this region causes both a sink and source and subsequently additional ionic fluxes of Al and S ions inside the domain. Nevertheless, the model is able to reproduce general trends reported in *e.g.* [56] concerning existence of a carbonated zone, a carbonation front, a dissolution front, and an unaffected zone. In particular, the formation and precipitation of $CaCO_3$ is associated with an initial reduction of the total pore volume. Due to the preferential deposition of $CaCO_3$ in smaller pores, owing to better water condensation [29], a shift in the pore size distribution towards smaller pore diameters is observed at *e.g.* 10 mm distance from the surface; see Figure 9. Reductions in cumulative pore volume determined by the presented modelling approach are in reasonable agreement with results presented in *e.g.* [16].

Similar as for the first case study, changes in the pore volume distribution can subsequently be used to determine the impact of carbonation on the mass transport as well as moisture storage capacity of the cement-based matrix. Figure 10 a) illustrates results concerning the moisture transport and indicates a considerable change in conductivity in the lower and higher moisture range. At saturation, a decrease

of around one order of magnitude is predicted by the modelling approach (for the chosen model parameters and assumptions), which is in good agreement with results reported in [16]. The model also predicts a decrease in moisture storage capacity over the complete moisture range (see Figure 10 b), which is in good agreement with results presented in [17]. The impact of pore volume changes on the ionic diffusion is illustrated in Figure 10 c), indicating a decrease in ionic diffusion over the complete moisture range due to alterations in the pore volume distribution as a result of changes in the phase assemblage.

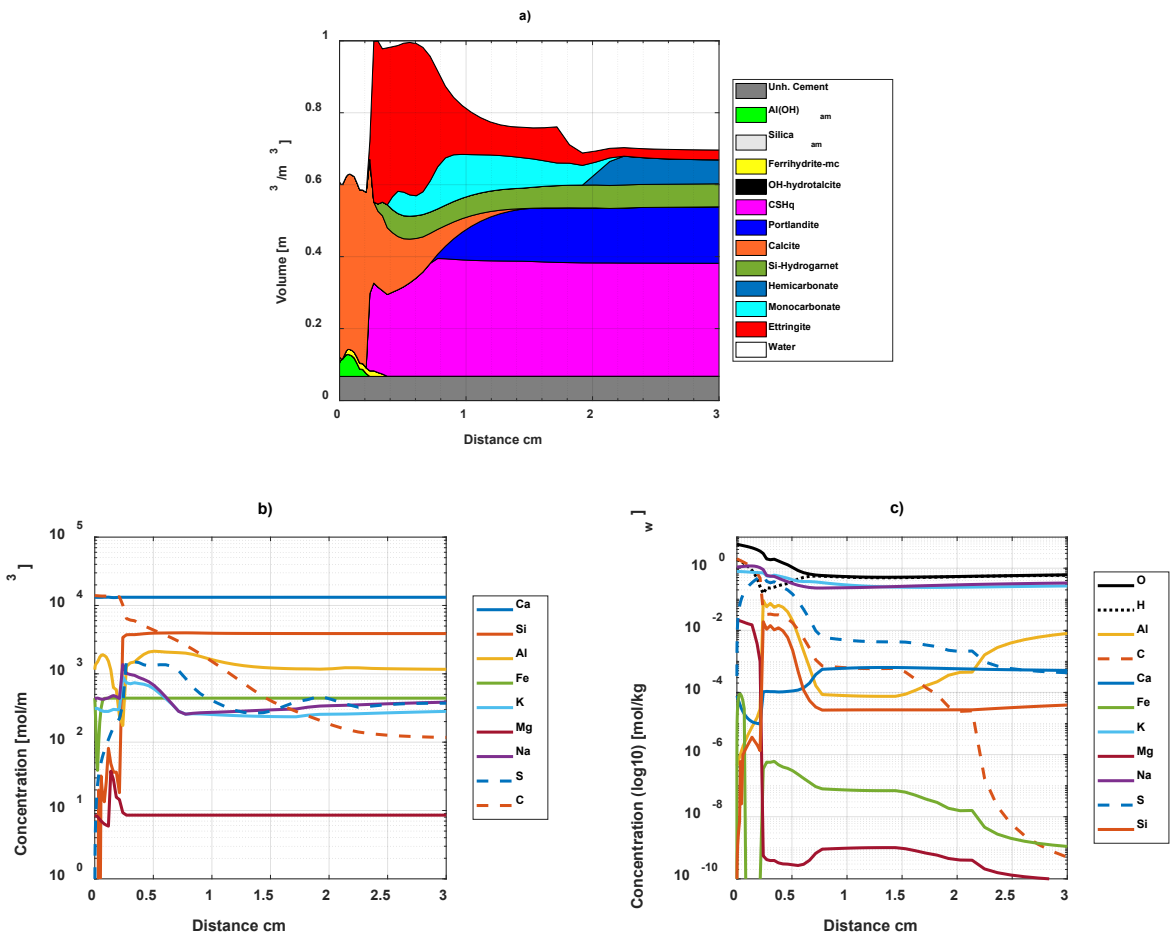

Figure 8: Model results of phase assemblage of cement-based matrix after 2 years of exposure to CO_2 containing solution: a) Solid phases, b) elemental composition, and c) total aqueous elemental concentrations.

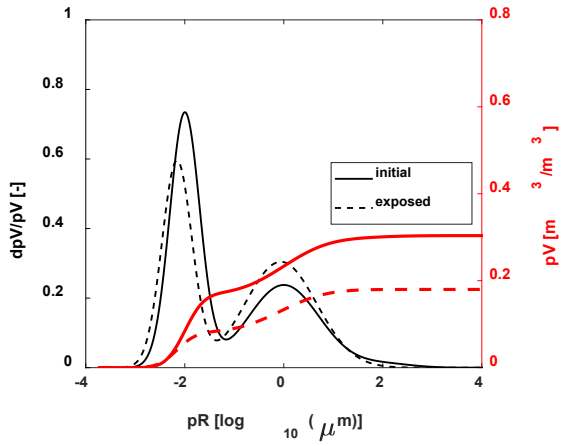

Figure 9: Change in pore size distribution and cumulative pore volume (normalized with respect to total pore volume) at 10 mm from the exposed node after 2 years of exposure to CO_2 containing solution.

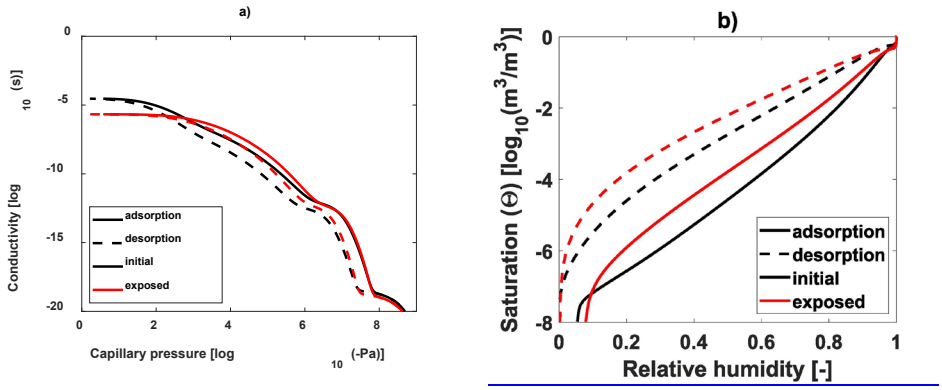

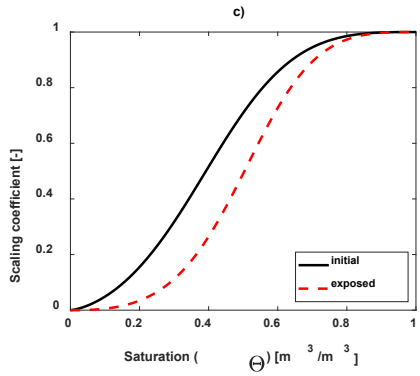

Figure 10: Impact of change in pore size distribution on a) moisture conductivity, b) moisture storage, and c) ionic diffusion at 10 mm from the exposed node after 2 years of exposure to CO_2 containing solution.

4 Discussion

Results of the presented case studies using the multi-physics modelling concept to account for the effect of microstructural changes (due to chemical reactions) on the mass transport properties show considerable changes in the composition of solid phases and pore solution, see Fig. 4 and 8. Apart from these changes, the chemical reactions lead to changes in the pore structure, resulting in significant changes in transport properties with particularly large impacts on the transport properties of (partially-) saturated systems (see *e.g.* Figure 11 for $\Theta \approx 0.4 - 0.7$). The changes in transport properties were dependent on the exposure and may lead to an increase or decrease in mass flow, see Fig. 6 and 10. Even gradual changes in microstructure, as observed for leaching and carbonation, resulted in highly non-linear (both spatial and temporal) changes in microstructure as well as mass transport properties, see Figure 11, which need to be accounted for as a whole.

While the presented concept is capable of capturing the governing mechanisms as well as general trends observed in experimental investigations, several challenges remain. In particular, testing and validation of the various first order approximations (concerning the shape parameter n_{sp} accounting for the serial-parallel connectivity of the pores, capillary sorption coefficient n_{cap}, the vapor diffusion resistance number μ_{dry}, and effective conductivity K_{eff}), entailed in the modelling approach to relate chemical reactions, pore structure changes, and mass transport are needed.

With respect to the complexity of changes in the pore size distribution, in particular localized changes need to be investigated and understood. At present, a less documented contribution of phase dissolution and formation to the pore size distribution is chosen, *i.e.* 70 % of the pore volume changes are attributed to gel pores, while 25 % and 5 % are attributed to capillary and macro pores, respectively. Commonly used techniques such as mercury intrusion porosimetry lack the ability to provide information on local variations of porosity. However, methods such as *e.g.* x-ray micro-tomography, may be applicable for detecting localized change in the pore volume distribution due to formation and dissolution of phases, see *e.g.* [58,59].

As a first order approximation, it assumed that pores are of cylindrical nature and that phases dissolve and form uniformly around the circumference of the pores leading to a reduction or increase in pore radius, and that changes in the pore radius relate by the power of four to the mass flow. Detailed information on the local distribution of phases and possible elemental zonation, *e.g.* by SEM EDS/ and µXRF [60,61] are needed to validate and improve assumptions on the phase assemblage upon exposure as well as provide spatial information on the formation and dissolution of individual phases.

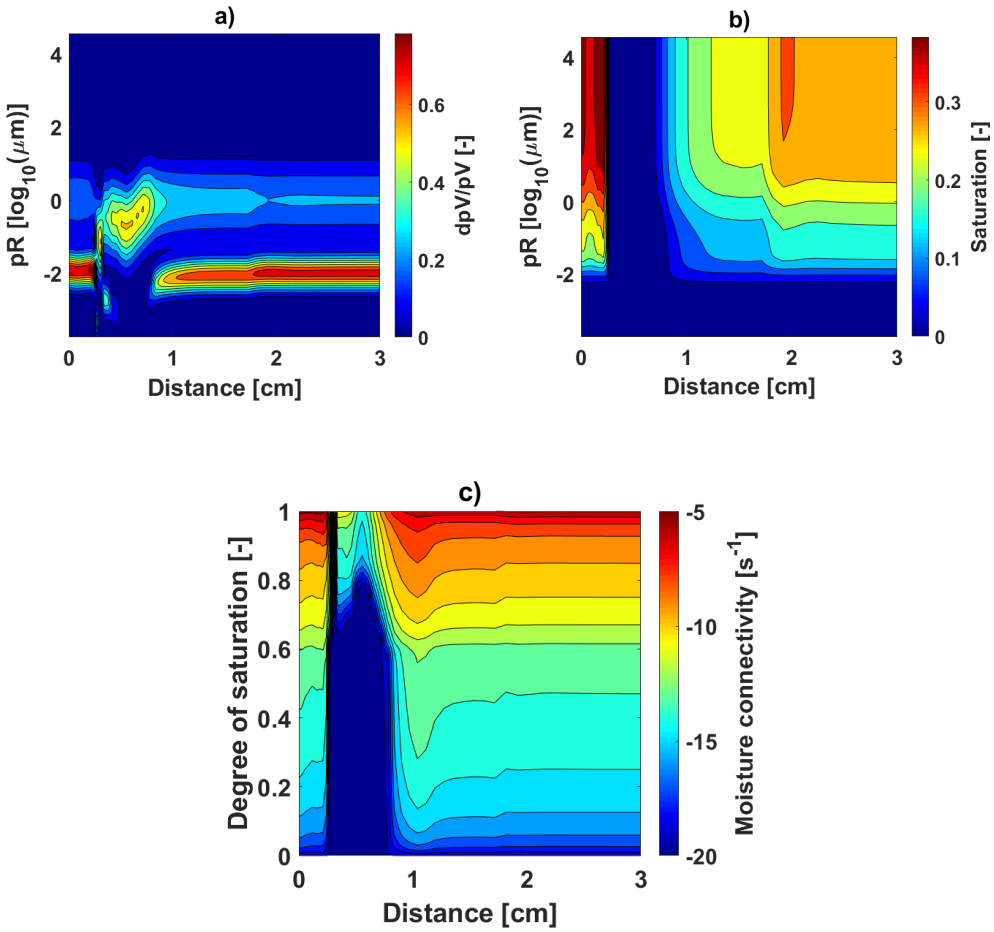

Figure 11: Change in a) pore size distribution, b) saturation-dependent ionic transport, and c) saturation-dependent moisture conductivity as function of depth for a cement-based material after 2 years of carbonation.

5 Conclusions

A concept that relates microstructural changes (*i.e.* changes in the pore structure and phase assemblage) of cement-based materials, chemical reactions, and mass transport was presented. Mass transport in cement-based materials along with chemical equilibrium between ions in the pore solution and solid hydrates was solved by an extended version of the Poisson-Nernst-Planck (PNP) system of equations,

in which the chemical equilibrium was solved by the external geochemical code IPHREEQC. Scaling functions based on a mechanistic modeling approach were used to relate phase changes and mass transport properties, taking into account the impact of both moisture content and the microstructure of porous media. To demonstrate the capability of the multi-physics modeling approach accounting for the effects of phase assemblage changes on the mass transport properties of cement-based materials, two case studies were presented, *i.e.* carbonation and leaching of a saturated system. Results of the modelling approach and comparison to experimental observations presented in the literature concluded the following:

- Microstructural changes, in particular changes in the pore size distribution, due to dissolution and formation of phases upon exposure can lead to considerable alterations of the mass transport properties of cement-based materials. Key to link changes in the pore volume distribution and mass transport is the chemical equilibrium as well as the simultaneous consideration of relations between microstructural changes and mass transport.
- Governing mechanisms and general trends are well represented by the developed modelling concept. However, improved understanding of the formation and changes of the pore structure with regard to transport related properties are required as well as further data for testing and validation of the model.
- The developed framework can be used to design experiments to investigate these mechanisms and refine first order approximations currently implemented.

Acknowledgements

The first author gratefully acknowledges financial support of the Danish Innovation Fond (1382-00054B) (Innovations Fonden) as a part of the "Green transition of cement and concrete production" (Grøn Beton II) project.

Appendix A

Table A 1: Overview of selected solid phases for the chemical equilibrium model. From [39].

	Chemical formula	Molar volume [cm^3/mol]	Molar mass [g/mol]
Equilibrium phases			
Anhydrite	$CaSO_4$	45.940	136.142
Gypsum	$CaSO_4\,(H2O)_2$	74.690	172.172
Lime	CaO	16.764	56.077
Portlandite	$Ca(OH)_2$	33.060	74.093
Calcite	$CaCO_3$	36.934	100.087
Hemicarbonate	$(CaO)_3\,Al_2O_3\,(CaCO_3)_{0.5}\,(CaO_2H2)_{0.5}\,(H_2O)_{11.5}$	284.515	564.459
Hydrotalcite	$Mg_4Al_2O_7\,(H_2O)_{10}$	220.200	443.332
Monocarbonate	$Ca_4Al_2CO_9\,(H_2O)_{11}$	261.958	568.449
Alum. hydroxide (am)	$Al(OH)_3$	31.956	78.004
Silica (am)	SiO_2	29.000	60.084
Ferrihydrite (am)	$FeO(OH)$	27.403	106.870
Solid solutions			
Si-Hydrogarnet			

$C_3AFS_{0.84}H_{4.32}$	$(AlFeO_3)\ (Ca_3O_3\ (SiO_2)_{0.84}\ (H_2O)_{4.32})$	145.5	427.4
$C_3FS_{0.84}H_{4.32}$	$(FeFeO_3)\ (Ca_3O_3\ (SiO_2)_{0.84}\ (H_2O)_{4.32})$	148.5	456.2
Ettringite			
Ettringite	$Ca_6Al_2(SO_4)_3(OH)_{12}\cdot 26H_2O$	216.8	382.3
SO_4-CO_3-AFt			
Tricarboaluminate(03)	$Ca_6Al_2(CO_3)_3(OH)_{12}\cdot 26H_2O$	216.8	382.3

Table A 2: End members in the C–S–H solid-solution model, after [41].

Solid solution	Chemical formula	Molar volume [cm^3/mol]	Molar mass [g/mol]
'CSHQ-TobH'	$(CaO)_{0.66}\ (SiO_2)\ (H_2O)_{1.5}$	55.0	124.5
'CSHQ-TobD'	$(CaO)_{0.83}\ (SiO_2)_{0.66}\ (H_2O)_{1.83}$	48.0	119.6
'CSHQ-JenH'	$(CaO)_{1.33}\ (SiO_2)\ (H_2O)_{2.16}$	76.0	173.9
'CSHQ-JenD'	$(CaO)_{1.5}\ (SiO_2)_{0.67}\ (H_2O)_{2.5}$	81.0	169.2
'KSiOH'	$((KOH)_{2.5}\ SiO_2\ H_2O)_{0.2}$	12.4	43.7
'NaSiOH'	$((NaOH)_{2.5}\ SiO_2\ H2O)_{0.2}$	10.5	35.6

Table A 3: Diffusion properties for ionic components in the numerical examples, from [23].

	D^i	A^i	z^i		D^i	A^i	z^i		D^i	A^i	z^i

OH^-	0.530	0,2253	-1	$H_3SiO_4^-$	0.107	0,0468	-1	$FeHSO_4^+$	0.072	0,0299	1
H^+	0.931	0,3958	1	H_4SiO_4	0.107	-	-	$Fe(OH)_4^-$	0.072	0,0299	-1
$Al(OH)_4^-$	0.504	0,2142	-1	Ca^{2+}	0.079	0	2	$Fe(OH)_3$	0.072	-	-
$Al(OH)_3$	0.504	-	-	Cl^-	0.203	0,0337	-1	$Fe(OH)_2^+$	0.072	0,0299	1
$Al(OH)_2^+$	0.504	0,2142	1	K^+	0.196	0,0405	1	$FeOH^{2+}$	0.072	0,0299	2
Al^{3+}	0.054	0,0229	3	KSO_4^-	0.107	0,0454	-1	$FeOH^+$	0.072	0,0299	1
$AlSO_4^+$	0.504	0,0442	1	KOH	0.196	-	-	Fe^{2+}	0.072	0,0299	2
$Al(SO_4)_2^-$	0.504	0,0442	-1	Mg^{2+}	0.071	0,0299	2	$NaSO_4^-$	0.618	0,0262	-1
$AlOH^{2+}$	0.504	0,0442	2	$MgSO_4$	0.071	0,0299	-	$NaOH$	0.133	-	-
$CaOH^+$	0.079	0,0337	1	$MgOH^+$	0.071	0,0299	1	$FeCl^+$	0.072	0,0299	1
$CaSO_4$	0.047	-	-	Na^+	0.133	0,0565	1	$FeSO_4$	0.072	-	-
$CaHSO_4^+$	0.047	0,0200	1	HSO_4^-	0.138	0,0589	-1	$H_2SiO_4^{2-}$	0.110	0,0468	-2
SO_4^{2-}	0.107	0,0455	-2								

D_i is the diffusion coefficient, A_i is the ion mobility, z_i is the valence of the ith ionic species

References

[1] T. Luping, J. Gulikers, On the mathematics of time-dependent apparent chloride diffusion coefficient in concrete, Cem. Concr. Res. 37 (2007) 589–595. doi:10.1016/j.cemconres.2007.01.006.

[2] T. Luping, Engineering expression of the ClinConc model for prediction of free and total chloride ingress in submerged marine concrete, Cem. Concr. Res. 38 (2008) 1092–1097. doi:10.1016/j.cemconres.2008.03.008.

[3] E. Samson, J. Marchand, Modeling the transport of ions in unsaturated cement-based materials, Comput. Struct. 85 (2007) 1740–1756. doi:10.1016/j.compstruc.2007.04.008.

[4] K. Maekawa, T. Ishida, T. Kishi, Multi-Scale Modeling of Structural Concrete, 2009.

[5] V. Baroghel-Bouny, T.Q. Nguyen, P. Dangla, Assessment and prediction of RC structure service life by means of durability indicators and physical/chemical models, Cem. Concr. Compos. 31 (2009) 522–534. doi:10.1016/j.cemconcomp.2009.01.009.

[6] M.M. Jensen, B. Johannesson, M.R. Geiker, Framework for reactive mass transport: Phase change modeling of concrete by a coupled mass transport and chemical equilibrium model, Comput. Mater. Sci. 92 (2014) 213–223. doi:10.1016/j.commatsci.2014.05.021.

[7] E. Samson, J. Marchand, Numerical Solution of the Extended Nernst–Planck Model, J. Colloid Interface Sci. 215 (1999) 1–8. doi:10.1006/jcis.1999.6145.

[8] B.F. Johannesson, Diffusion of a mixture of cations and anions dissolved in water, Cem. Concr. Res. 29 (1999) 1261–1270. doi:10.1016/S0008-8846(99)00114-3.

[9] O. Kolditz, S. Bauer, L. Bilke, N. Böttcher, J.O. Delfs, T. Fischer, U.J. Görke, T. Kalbacher, G. Kosakowski, C.I. McDermott, C.H. Park, F. Radu, K. Rink, H. Shao, H.B. Shao, F. Sun, Y.Y. Sun, A.K. Singh, J. Taron, M. Walther, W. Wang, N. Watanabe, Y. Wu, M. Xie, W. Xu, B. Zehner, OpenGeoSys: An open-source initiative for numerical simulation of thermo-hydro-mechanical/chemical (THM/C) processes in porous media, Environ. Earth Sci. 67 (2012) 589–599. doi:10.1007/s12665-012-1546-x.

[10] B. Johannesson, Development of a Generalized Version of the Poisson– Nernst–Planck Equations Using the Hybrid Mixture Theory: Presentation of 2D Numerical Examples, Transp. Porous Media. 85 (2010) 565–592. doi:10.1007/s11242-010-9578-8.

[11] D.L. Parkhurst, C.A.J. Appelo, Description of Input and Examples for PHREEQC Version 3—A Computer Program for Speciation, Batch-Reaction, One-Dimensional Transport, and Inverse Geochemical Calculations, 2013. https://pubs.usgs.gov/tm/06/a43/.

[12] G.A. Scheffler, R. Plagge, A whole range hygric material model: Modelling liquid and vapour transport properties in porous media, Int. J. Heat Mass Transf. 53 (2010) 286–296. doi:10.1016/j.ijheatmasstransfer.2009.09.030.

[13] G. Scheffler, Validation of Hygrothermal Material Modelling Under Consideration of the Hysteresis of Moisture Storage, Ph.D. Thesis, TU Dresden, 2008.

[14] C. Galle, H. Peycelon, P. Le Bescop, Effect of an accelerated chemical degradation on water permeability and pore structure of cement-based materials, Adv. Cem. Res. 16 (2004) 105–114. doi:10.1680/adcr.16.31.105.41515.

[15] Q.T. Phung, N. Maes, D. Jacques, G. De Schutter, G. Ye, Investigation of the changes in microstructure and

transport properties of leached cement pastes accounting for mix composition, Cem. Concr. Res. 79 (2016) 217–234. doi:10.1016/j.cemconres.2015.09.017.

[16] Q.T. Phung, N. Maes, D. Jacques, E. Bruneel, I. Van Driessche, G. Ye, G. De Schutter, Effect of limestone fillers on microstructure and permeability due to carbonation of cement pastes under controlled CO2 pressure conditions, Constr. Build. Mater. 82 (2015) 376–390. doi:10.1016/j.conbuildmat.2015.02.093.

[17] Y.F. Houst, F.H. Wittmann, Influence of porosity and water content on the diffusivity of CO2 and O2 through hydrated cement paste, Cem. Concr. Res. 24 (1994) 1165–1176. doi:10.1016/0008-8846(94)90040-X.

[18] O. Zienkiewicz, The Finite Element Method: its Basis and Fundamentals, Elsevier, 2013. doi:10.1016/C2009-0-24909-9.

[19] M.M. Jensen, A Coupled Transport and Chemical Model for Durability Predictions of Cement Based Materials, PhD thesis, Technical University of Denmark, 2014.

[20] M. Addassi, Transport in concrete with new CO2-reduced cements -Reactive Transport Model for Durability Estimations, PhD thesis, Technical University of Denmark, 2018.

[21] A. Michel, V.M. Meson, H. Stang, M.R. Geiker, M. Lepech, Coupled mass transport , chemical , and mechanical modelling in cementitious materials : A dual-lattice approach, in: R. Caspeele, L. Taerwe, D.M. Frangepol (Eds.), Life Cycle Anal. Assess. Civ. Eng. Towar. an Integr. Vis. Proc. Sixth Int. Symp. Life-Cycle Civ. Eng. (IALCCE 2018), CRC PRESS-TAYLOR & FRANCIS GROUP, 2018: pp. 965–972.

[22] Y. Hosokawa, K. Yamada, B. Johannesson, L.O. Nilsson, Development of a multi-species mass transport model for concrete with account to thermodynamic phase equilibriums, Mater. Struct. Constr. 44 (2011) 1577–1592. doi:10.1617/s11527-011-9720-2.

[23] M.M. Jensen, K. De Weerdt, B. Johannesson, M.R. Geiker, Use of a multi-species reactive transport model to simulate chloride ingress in mortar exposed to NaCl solution or sea-water, Comput. Mater. Sci. 105 (2015) 75–82. doi:10.1016/j.commatsci.2015.04.023.

[24] H. Janssen, B. Blocken, J. Carmeliet, Conservative modelling of the moisture and heat transfer in building components under atmospheric excitation, Int. J. Heat Mass Transf. 50 (2007) 1128–1140.

doi:10.1016/j.ijheatmasstransfer.2006.06.048.

[25] J.R. Philip, D.A. De Vries, Moisture movement in porous materials under temperature gradients, Trans. Am. Geophys. Union. 38 (1957) 222. doi:10.1029/TR038i002p00222.

[26] F.A.L.A.L. Dullien, Porous Media Fluid Transport and Pore Structure, 2nd Editio, Academic Press, Inc., San Diego, 1991. doi:https://doi.org/10.1016/C2009-0-26184-8.

[27] J. Bear, Y. Bachmat, Introduction to modeling of transport phenomena in porous media, Kluwer Academic Publishers, 1991.

[28] J. Grunewald, P. Häupl, M. Bomberg, Towards an Engineering Model of Material Characteristics for Input to Ham Transport Simulations - Part 1: An Approach, J. Build. Phys. 26 (2003) 343–366. doi:10.1177/1097196303026004002.

[29] M.T. \hboxvan Genuchten, A Closed Form Equation for Predicting the Hydraulic Conductivity of Unsaturated Soils, Soil Sci. Soc. Am. J. 44 (1980) 892–898. http://findit.dtu.dk/en/catalog/2367616338 (accessed August 21, 2018).

[30] W. Durner, Hydraulic conductivity estimation for soils with heterogeneous pore structure, Water Resour. Res. 30 (1994) 211–223. doi:10.1029/93WR02676.

[31] S. Roels, J. Elsen, J. Carmeliet, H. Hens, Characterisation of pore structure by combining mercury porosimetry and micrography, Mater. Struct. Constr. 34 (2001) 76–82. doi:10.1617/13555.

[32] J. Adolphs, M.J. Setzer, P. Heine, Changes in pore structure and mercury contact angle of hardened cement paste depending on relative humidity, Mater. Struct. Constr. 35 (2002) 477–486. doi:10.1007/BF02483135.

[33] N.T. Burdine, Relative Permeability Calculations From Pore Size Distribution Data, J. Pet. Technol. 5 (1953) 71–78. doi:10.2118/225-G.

[34] B. Lothenbach, T. Matschei, G. Möschner, F.P. Glasser, Thermodynamic modelling of the effect of temperature on the hydration and porosity of Portland cement, Cem. Concr. Res. 38 (2008) 1–18. doi:10.1016/j.cemconres.2007.08.017.

[35] M. Balonis, F.P. Glasser, The density of cement phases, Cem. Concr. Res. 39 (2009) 733–739. doi:10.1016/j.cemconres.2009.06.005.

[36] B.Z. Dilnesa, B. Lothenbach, G. Le Saout, G. Renaudin, A. Mesbah, Y. Filinchuk, A. Wichser, E. Wieland, Iron in carbonate containing AFm phases, Cem. Concr. Res. 41 (2011) 311–323. doi:10.1016/j.cemconres.2010.11.017.

[37] R. Schirmer, Die Diffusionszahl von Wasserdampf-Luft-Gemischen und die Verdampfungsgeschwindigkeit, VDI-Verlag, 1938.

[38] Y. Mualem, A new model for predicting the hydraulic conductivity of unsaturated porous media, Water Resour. Res. 12 (1976) 513–522. doi:10.1029/WR012i003p00513.

[39] B. Lothenbach, D.A. Kulik, T. Matschei, M. Balonis, L. Baquerizo, B. Dilnesa, G.D. Miron, R.J. Myers, Cemdata18: A chemical thermodynamic database for hydrated Portland cements and alkali-activated materials, Cem. Concr. Res. 115 (2019) 472–506. doi:10.1016/j.cemconres.2018.04.018.

[40] T. Thoenen, W. Hummerl, U. Berner, E. Curti, The PSI/Nagra Chemical Thermodynamic Database 12/07, Villigen, Switzerland, 2014. https://www.psi.ch/les/DatabaseEN/PSI-Bericht 14-04_final_druckerei.pdf.

[41] D.A. Kulik, Improving the structural consistency of C-S-H solid solution thermodynamic models, Cem. Concr. Res. 41 (2011) 477–495. doi:10.1016/j.cemconres.2011.01.012.

[42] T. De Larrard, S. Poyet, M. Pierre, F. Benboudjema, P. Le Bescop, J.B. Colliat, J.M. Torrenti, Modelling the influence of temperature on accelerated leaching in ammonium nitrate, Eur. J. Environ. Civ. Eng. 16 (2012) 322–335. doi:10.1080/19648189.2012.675175.

[43] V.H. Nguyen, B. Nedjar, J.M. Torrenti, Chemo-mechanical coupling behaviour of leached concrete. Part II: Modelling, Nucl. Eng. Des. 237 (2007) 2090–2097. doi:10.1016/j.nucengdes.2007.02.012.

[44] H. Yang, L. Jiang, Y. Zhang, Q. Pu, Y. Xu, Predicting the calcium leaching behavior of cement pastes in aggressive environments, Constr. Build. Mater. 29 (2012) 88–96. doi:10.1016/j.conbuildmat.2011.10.031.

[45] S. Poyet, P. Le Bescop, M. Pierre, L. Chomat, C. Blanc, Accelerated leaching of cementitious materials using ammonium nitrate (6M): Influence of test conditions, Eur. J. Environ. Civ. Eng. 16 (2012) 336–351.

doi:10.1080/19648189.2012.667712.

[46] C. Perlot, J. Verdier, M. Carcassés, Influence of cement type on transport properties and chemical degradation: Application to nuclear waste storage, Mater. Struct. Constr. 39 (2006) 511–523. doi:10.1617/s11527-005-9020-9.

[47] K. De Weerdt, D. Orsáková, A.C.A. Müller, C.K. Larsen, B. Pedersen, M.R. Geiker, Towards the understanding of chloride profiles in marine exposed concrete, impact of leaching and moisture content, Constr. Build. Mater. 120 (2016) 418–431. doi:10.1016/j.conbuildmat.2016.05.069.

[48] B. Šavija, M. Luković, Carbonation of cement paste: Understanding, challenges, and opportunities, Constr. Build. Mater. 117 (2016) 285–301. doi:10.1016/j.conbuildmat.2016.04.138.

[49] M. Thiery, G. Villain, P. Dangla, G. Platret, Investigation of the carbonation front shape on cementitious materials: Effects of the chemical kinetics, Cem. Concr. Res. 37 (2007) 1047–1058. doi:10.1016/j.cemconres.2007.04.002.

[50] G.W. Groves, D.I. Rodway, I.G. Richardson, The carbonation of hardened cement pastes, Adv. Cem. Res. 3 (1990) 117–125. doi:10.1680/adcr.1990.3.11.117.

[51] N. Hyvert, A. Sellier, F. Duprat, P. Rougeau, P. Francisco, Dependency of C-S-H carbonation rate on CO2pressure to explain transition from accelerated tests to natural carbonation, Cem. Concr. Res. 40 (2010) 1582–1589. doi:10.1016/j.cemconres.2010.06.010.

[52] Z. Shi, B. Lothenbach, M.R. Geiker, J. Kaufmann, A. Leemann, S. Ferreiro, J. Skibsted, Experimental studies and thermodynamic modeling of the carbonation of Portland cement, metakaolin and limestone mortars, Cem. Concr. Res. 88 (2016) 60–72. doi:10.1016/j.cemconres.2016.06.006.

[53] T.F. Sevelsted, J. Skibsted, Carbonation of C-S-H and C-A-S-H samples studied by13C,27Al and29Si MAS NMR spectroscopy, Cem. Concr. Res. 71 (2015) 56–65. doi:10.1016/j.cemconres.2015.01.019.

[54] C.A. García-González, A. Hidalgo, C. Andrade, M.C. Alonso, J. Fraile, A.M. López-Periago, C. Domingo, Modification of composition and microstructure of Portland cement pastes as a result of natural and supercritical carbonation procedures, Ind. Eng. Chem. Res. 45 (2006) 4985–4992. doi:10.1021/ie0603363.

[55] V.T. Ngala, C.L. Page, Effects of carbonation on pore structure and diffusional properties of hydrated cement

pastes, Cem. Concr. Res. 27 (1997) 995–1007. doi:10.1016/S0008-8846(97)00102-6.

[56] G. Rimmelé, V. Barlet-Gouédard, O. Porcherie, B. Goffé, F. Brunet, Heterogeneous porosity distribution in Portland cement exposed to CO2-rich fluids, Cem. Concr. Res. 38 (2008) 1038–1048. doi:10.1016/j.cemconres.2008.03.022.

[57] P.H.R. Borges, J.O. Costa, N.B. Milestone, C.J. Lynsdale, R.E. Streatfield, Carbonation of CH and C-S-H in composite cement pastes containing high amounts of BFS, Cem. Concr. Res. 40 (2010) 284–292. doi:10.1016/j.cemconres.2009.10.020.

[58] X. Yu, Y. Fu, S. Lu, Characterization of the pore structure and cementing substances of soil aggregates by a combination of synchrotron radiation X-ray micro-computed tomography and scanning electron microscopy, Eur. J. Soil Sci. 68 (2017) 66–79. doi:10.1111/ejss.12399.

[59] K. Wan, Q. Xu, Local porosity distribution of cement paste characterized by X-ray micro-tomography, Sci. China Technol. Sci. 57 (2014) 953–961. doi:10.1007/s11431-014-5513-5.

[60] M. Khanzadeh Moradllo, B. Sudbrink, Q. Hu, M. Aboustait, B. Tabb, M.T. Ley, J.M. Davis, Using micro X-ray fluorescence to image chloride profiles in concrete, Cem. Concr. Res. 92 (2017) 128–141. doi:10.1016/j.cemconres.2016.11.014.

[61] U.H. Jakobsen, K. De Weerdt, M.R. Geiker, Elemental zonation in marine concrete, Cem. Concr. Res. 85 (2016) 12–27. doi:10.1016/j.cemconres.2016.02.006.